Universal Heliophysical Processes
Proceedings IAU Symposium No. 257, 2008
N. Gopalswamy & D. F. Webb, eds.

doi:10.1017/S1743921309029159

The maximum magnetic flux in an active region

George Livadiotis[a,b,1] **and Xenophon Moussas**[b,2]

[a]Space Science and Engineering Division, Southwest Research Institute,
San Antonio, TX 78238, US
[b]Department of Astrophysics, Astronomy and Mechanics, Faculty of Physics,
National and Capodistrian University of Athens,
Panepistimiopolis, GR 15784, Zografos, Athens, Greece
[1]email: glivadiotis@swri.edu; glivad@phys.uoa.gr [2]email: xmoussas@phys.uoa.gr

Abstract. The Photometric-Magnetic Dynamical model handles the evolution of an individual sunspot as an autonomous nonlinear, though integrable, dynamical system. The model considers the simultaneous interplay of two different interacted factors: The photometric and magnetic factors, respectively, characterizing the evolution of the sunspot visible area A on the photosphere, and the simultaneous evolution of the sunspot magnetic field strength B. All the possible sunspots are gathered in a specific region of the phase space (A, B). The separatrix of this phase space region determines the upper limit of the values of sunspot area and magnetic strength. Consequently, an upper limit of the magnetic flux in an active region is also determined, found to be $\approx 7.23 \times 10^{23}$ Mx. This value is phenomenologically equal to the magnetic flux concentrated in the totality of the granules of the quite Sun. Hence, the magnetic flux concentrated in an active region cannot exceed the one concentrated in the whole photosphere.

Keywords. Sun: sunspots; activity; magnetic fields; granulation

1. Introduction

During the last sixty years, the phenomenon of the decay phase of sunspots has been a highly controversial issue within the heliophysical community. This involves establishing the exact mathematical expression of the area decay rate of the sunspots. The particular mathematical formula of the decay rate, also called a decay law, is a key point for understanding the specific underlying physical mechanism of sunspot dissolution.

Previous theoretical models, made for describing the sunspot evolution, had the common characteristic of originating in Magnetohydrodynamical equations, constructed after suitable simplifications and modifications. However, each one focuses only on the decay phase of sunspots, resulting to a specific decay law, which indeed, is supported by parts of the observational data.

In such a way, since today three decay laws have prevailed: (i) The linear decay law, $\dot{A} = -w$, where the area decay rate is negative constant ($w > 0$). (ii) The parabolic decay law, $\dot{A} \propto -\sqrt{A}$, exhibiting a slower decay rate than the linear law, because of the positive constant second derivative of area with respect to time, $\ddot{A} > 0$. Finally, (iii) the exponential decay law, $\dot{A} \propto -A$, characterized by a faster decay rate than the linear law (Livadiotis & Moussas (2007), c.f. Introduction). (The dot denotes the derivative with respect to time t.)

On the other hand, the Photometric-Magnetic Dynamical (PhMD) model, introduced by Livadiotis & Moussas (2007), has its own origin, constructed considering several

meaningful physical terms. It considers the simultaneous interplay of two different interacted factors: The photometric one, characterizing the evolution of the sunspot visible area A on the photosphere; the magnetic factor, characterizing the simultaneous evolution of the sunspot magnetic field strength B.

In relevance to the previous models, we mention that the PhMD model first of all, describes the whole sunspot lifetime, either the growth or decay phases. It reproduces all the three decay laws: Each decay law is applicable at a different time of the decay phase. Moreover, it predicts the characteristic numerical features of each decay law, as found from the observational data.

In addition, the PhMD model, among others, predicts (i) the distribution of the maximum sunspot areas, (ii) an estimation of the granules mean dimensions, (iii) an upper limit for the maximum values of sunspot area and magnetic strength, and (iv) an upper limit for the maximum value of magnetic flux concentrated in an active region. Here we will discuss the issue of upper limits. We stress that the model is an integrable two-dimensional dynamical system. However, its non-integrable version, that is the perturbed photometric magnetic dynamical model has also been investigated (Livadiotis & Moussas 2008).

2. Construction of the model

The model is formulated by a two-dimensional dynamical system, whereby the two time-dependent functions are the photospheric sunspot area $A(t)$, and its magnetic field strength $B(t)$, characterizing the sunspot as a whole.

$$\begin{aligned} \dot{A} &= -a_1(A - A_G) + a_2(B^2 - {B_G}^2) \\ \dot{B} &= -b_{11}A + b_{12} - b_{13}\sqrt{A} + b_2(B - B_G) \ . \end{aligned} \tag{2.1}$$

As we can see, there are five different additive physical terms, explained below:

The first term, $a_2(B^2 - {B_G}^2)$, yields the creation mechanism of the sunspot. This involves magnetic flux fragments such as those of pores or of other elementary magnetic microstructures, erupting from below the photosphere due to the magnetic buoyancy, while their accumulated smaller flux tubes coalesce into a main core of a larger flux tube. The magnetic buoyancy is a component being proportional to B^2, thus the same holds for the first term, being mentioned.

The next two terms, $-b_{11}A + b_{12}$, $-b_{13}\sqrt{A}$, constitute what we call "collar flow" (Fig. 1a), that is the exchange of inflow and outflow of magnetic flux, respectively (Solanki 2003). Thus, magnetic flux can inflow either through the entire sunspot projected area A, emerging from the solar interior, or through locally specified regions with sufficiently smaller dimensions compared to those of sunspot. On the other hand, magnetic flux can outflow sideways through the area of sunspots, that is a component proportional to the square root of A.

The other two components, $-a_1(A - A_G)$, $+b_2(B - B_G)$, constitute the negative and positive feedbacks, respectively, characterizing the resistance to the area increasing due to the creation mechanism and the magnetic strength decreasing due to the magnetic outflow.

Therefore, the inflow and outflow are combined in order to form the collar flow, which together with the feedbacks, help to stabilized the sunspot. We underline that the model considers that a sunspot does not only maintain its existence, but also evolves during its whole lifetime, by interacting with the simultaneously evolved magnetic field.

https://doi.org/10.1017/S1743921309029159 Published online by Cambridge University Press

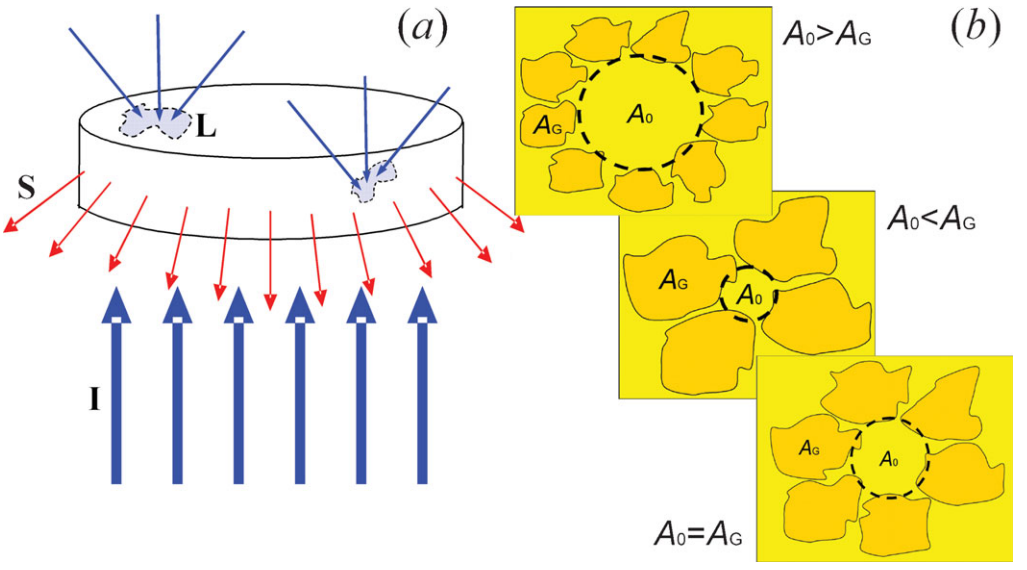

Figure 1. (a) The inflow and outflow, combined, form the well known collar flow, that together with the feedbacks, helps to stabilize the sunspot. The PhMD model considers that a sunspot does not only maintain its existence, but also evolves during its whole lifetime, by interacting with the simultaneously evolved magnetic field. (I: solar interior inflow, L: local inflow, S: sideways outflow.) (b) Scheme of granules arrangement: low density arrangement $A_0 > A_G$; high density arrangement $A_0 < A_G$; initial equilibrium $A_0 = A_G$.

The small characteristic scales A_G, and B_G, are related to the granules, as we shall see further below.

3. Granules characteristic scales

Here we arrive at an interpretation of the area characteristic scales A_G, and B_G. This arises considering the geometric arrangement of granules.

The procedure of magnetic flux tubes coalescence initially takes place in the intermediate space between adjacent granules. Therefore, this is the space, being disposed to the sunspot initial area, A_0.

Now, suppose that granules happens to be distributed in a locally low density arrangement, namely, the initial sunspot area A_0 is larger than the granule area A_G (Fig. 1b). Then, the system shall be spontaneously driven to a higher density arrangement. The enclosed area is compressed, being opposed to the emergence of magnetic elements from below the photosphere, leading to a resistance on the area initial growth, being proportional to the difference between the initial sunspot area A_0 and the granule area A_G.

Obviously, in the opposite case of locally high density granules arrangement, $A_0 < A_G$, the physical system is spontaneously driven to a lower density arrangement, giving advance to the sunspot creation, exhibiting thus, a negative resistance.

The case of neither high nor low density arrangement is thought to express an initial equilibrium, formulated by the initial conditions of zeroth area growth rate and zeroth resistance, that is the initial area being equal to that of the surrounding granules, $A_0 = A_G$. Consequently, we also have that the initial magnetic strength B_0 is equal to the respective scale B_G.

https://doi.org/10.1017/S1743921309029159 Published online by Cambridge University Press

4. Normalized dynamical system

By considering proportionality relations between the functions $A(t)$, $B(t)$, and their respective initial values, A_G, B_G, we can define the new dimensionless variables $x(t) \equiv \frac{A(t)}{A_G}$ and $y(t) \equiv \frac{B(t)}{B_G}$. Then, the system Eq. (2.1), can be rewritten as follows:

$$\begin{aligned} \dot{A} &= a_1[-x + q(y^2 - 1)] \\ \dot{B} &= b_2[p_1 x - p_2\sqrt{x} + y + m] \ . \end{aligned} \tag{4.1}$$

The physical meaning of the new parameters is inherited from the old ones, namely,

- $a_1 = b_2$ yields a characteristic time scale $\tau \equiv a_1 t$,
- $q = +\frac{1}{y^2-1}(\frac{dx}{d\tau})_C$ is related to the sunspot creation mechanism (C: coalescence),
- $p_1 = +\frac{1}{x}(\frac{dy}{d\tau})_I$ characterizes the inflow of the magnetic flux through the solar interior (I: interior),
- $m = +(\frac{dy}{d\tau})_L$: characterizes the inflow through the small local regions (L: local regions),
- $p_2 = -\frac{1}{\sqrt{x}}(\frac{dy}{d\tau})_S$ characterizes the outflow of the magnetic flux through the sunspot boundary (S: sideways area).

Furthermore, we stress that the dynamical system is conservative, $\vec{\nabla}[\dot{x}(x,y), \dot{y}(x,y)] = 0$, since the condition a_1 being equal to b_2, leads to a closed phase space curve, that is the only phase space curve with physical meaning. Indeed, for $a_1 > b_2$, phase space trajectories converge to a sink, describing a sunspot of infinite lifetime. On the other hand, for $a_1 < b_2$, phase space trajectories diverge to infinity, describing sunspots of infinite dimensions. Both cases are physically unacceptable, and thus, we conclude with the condition $a_1 = b_2$.

Therefore, the Hamiltonian constraint is given by the expression,

$$H(x,y) = \frac{a_1}{3}\left\{qy^3 + 3(1-q-x)y + 2\left[-\frac{3}{4}p_1(x^2-1) + p_2(x^{\frac{3}{2}}-1) - \frac{3}{2}m(x-1) + q\right]\right\}, \tag{4.2}$$

while sunspots found to be described by zeroth constraint value, $H(x,y) = H(x_0 = 1, y_0 = 1) = 0$.

We remark that the normalized expression of the system Eq.(4.1) shall remain invariant if we adopt a common functional type for the positive and negative feedbacks involved in Eq. (2.1), namely, $a_{11}(A - A_G) + a_{12}(B - B_G)$ instead of $a_1(A - A_G)$, and $b_{21}(A - A_G) + b_{22}(B - B_G)$ instead of $b_2(B - B_G)$. However, the normalized dimensionless variables have to be defined by $x(t) \equiv \frac{A(t)}{A_G}$ and $y(t) \equiv \lambda\frac{B(t)}{B_G} - \lambda - 1$, where the new parameter $\lambda \equiv (\frac{a_{12}}{2a_2 B_G} - 1)^{-1}$ is encrypted in the expression of y. (In similar way that the other parameters A_G and B_G are encrypted in the expressions of x and y.) Then, A_G and B_G, λ, have to be respectively taken into account when we reverse the problem and we want to find $A(t)$ and $B(t)$ in terms of $x(t)$ and $y(t)$.

5. Results: The fitting of the model and the predicted decay laws

The fitting of the model to the observational data was derived in three different ways: First, we compared the model predictions with the observational data referring to one single sunspot. In such a way, we selected several compact individual sunspots where the model predicted curve of area $A(t)$ was fitted to the respective photometric light curves, as shown in Figs. 2a,b for the (RGO-UASF/NOAA) AR1485104 and AR1488603, respectively. Second, we dealt with the fitting of the model predicted phase space curves

https://doi.org/10.1017/S1743921309029159 Published online by Cambridge University Press

$[A(t), \dot{A}(t)]$ to the statistically modified forty three respective pairs characterizing the totality of large sunspots $A > 35$ MSH (Millionths of Solar Hemisphere), as shown in Fig. 2c. The statistical analysis, being utilized here, was by Hathaway & Choudhary (2005). They arranged all the decay rates of sunspots into forty three bins of areas, and then, they calculated the mean and the standard deviation of the decay rate of each bin. (This statistical manipulation concerns 24000 values of decay rates from the daily observational data of Royal Greenwich Observatory in 1874-1976, that have been analyzed.) We mentioned that there was another kind of fitting, that is the fitting of the model predicted distribution of the maximum sunspot areas to the respective observational one, found to be a Log-Normal distribution (Martínez Pillet *et al.* 1993). (For further details, see: Livadiotis & Moussas 2007.)

One of the significant results of the fitting was that three model parameters remain constant, having for all the sunspots the same fixed value. Namely, $q = 310 \pm 10, p_1 = (1.85 \pm 0.10) \times 10^{-3}, m = 4.90 \pm 0.03$. On the other hand, there are also variant parameters, such as p_2, a_1, A_G, B_G. However, the only variant parameter, that affects the $[x(t), y(t)]$ trajectories for each sunspot, is the outflow p_2.

In Fig. 2d we depict the evolution of a large sunspot along the trajectories $[A(t), \dot{A}(t)]$. The enlarged panel illustrates the decay phase. We observe the "sub-phase" where the linear decay law is applicable (indicated as L), and also for the parabolic (as P), and the exponential (as E) decay laws. Also, notice the divergence from exponential law (indicated as dE), which has recently been established from observations. (Compare with Fig. 2c.) In addition, we remark that the model predicts the correct numerical features of each of the three decay laws, as found from observations (Livadiotis & Moussas 2007).

We stress the fact that even though the model predicted evolution of sunspot area (photometric evolution) has been suitably adjusted to the observational data, the magnetic evolution has not yet been fitted, since the solar magnetic observational data are

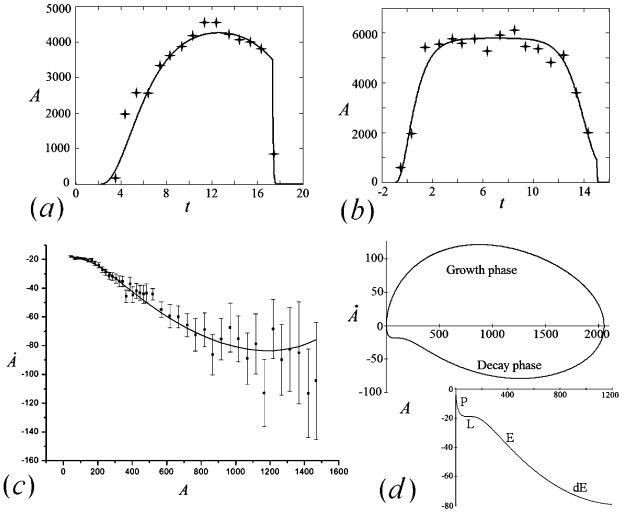

Figure 2. Fitting of sunspots (RGO-USAF/NOAA) AR1485104 (a), AR1488603 (b). (c) Fitting of the model predicted curve $[A(t), \dot{A}(t)]$ (solid line) with the mean decay rates derived from Hathaway & Choudhary (2005). (d) Evolution of a large sunspot along the trajectories $[A(t), \dot{A}(t)]$. (L: linear, P: parabolic, and E: exponential decay laws; dE: divergence from exponential decay law.)

https://doi.org/10.1017/S1743921309029159 Published online by Cambridge University Press

rather poor and inadequate. Nevertheless, the values of B_G and λ have been estimated in the case of large sunspots, that is $B_G \approx 3100$ G and $\lambda \approx 25$. (For details, see: Livadiotis & Moussas 2009.)

6. Phase space trajectories $[x(t), y(t)]$

The various trajectories $[x(t), y(t)]$ can be represented in the phase space diagram as iso-Hamiltonians. Namely, each trajectory is specified by its Hamiltonian constraint value, but all of them are characterized by a fixed value of the outflow p_2. On the other hand, however, trajectories can be represented as iso-outflows. Namely, each trajectory is specified by its outflow p_2 value, but all of them are characterized by a fixed value of the Hamiltonian constraint.

The iso-outflows phase space representation is preferred, since the totality of sunspots are characterized by one single fixed value of Hamiltonian constraint, namely $H(x, y) = 0$, derived from the initial equilibrium condition, described in Sec. 3. Even if we adopt the common functional type of feedbacks, described in Sec. 4, the initial equilibrium condition remains, namely, $A_0 = A_G$, $\dot{A}_0 = 0$, leading to $y_0 = 1$. Then, we readily derive that $x_0 = 1$, $y_0 = 1$, resulting to $H(x, y) = 0$.

This phase space representation is illustrated in Fig. 3, whereby the totality of sunspots can be found in the grey region of the trajectories. This is limited by the peculiar stable point S_1 and by the unstable point U_2. All the trajectories expand, as p_2 decreases. The outflow maximum value, $p_{2,Max} = p_1 + 1 + m \simeq 5.90185$, corresponds to the trivial single point trajectory, that is S_1, while the outflow minimum value, $p_{2,Min} \simeq 0.26284686\ldots$, corresponds to the most expanded trajectory, that passes through U_2.

Hence, the largest value of the maximum normalized area x_{max} corresponds to the outflow minimum value, $p_{2,Min} \simeq 0.26284686\ldots$, and that is the upper limit of the normalized areas, found to be of about $x_{UpLim} = 5700$.

Given the value of the initial area, that is of the area of the initially surrounding granules, we can arrive at the upper limit of the sunspot areas. Therefore, by utilizing the maximum area attained by granules, that is $A_{G,max} = 1.1$ MSH (Foukal 2004), we retrieve the sunspot area upper limit, namely, $A_{UpLim} = A_{G,max} \cdot x_{UpLim}$, hence,

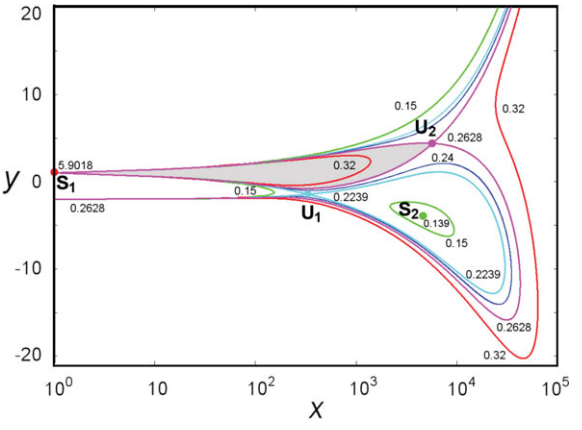

Figure 3. The phase space portrait represented by the iso-outflow curves. ($S_{1,2}$: stable, $U_{1,2}$: unstable fixed points. The Hamiltonian constraint is zero. The outflow p_2 values are indicated.)

https://doi.org/10.1017/S1743921309029159 Published online by Cambridge University Press

$A_{UpLim} = 6200 \pm 400$ MSH. (The errors of the fixed values parameters propagate the error of the upper limit areas.) We note that the peculiar case of the year 1947 is characterized by extremely large sunspots with areas bounded by the estimated upper limit. The light-curve of the largest ever sunspot, that appeared on April 3, 1947, is shown in Fig. 2b.

The unstable point U_2 yields also the upper limit for the normalized magnetic strength y, that is $y_{UpLim} = 4.404$. Given the values of $B_{G,max} \approx 3100$ G and $\lambda_{max} \approx 25$ that correspond to large sunspots, we arrive at the sunspot magnetic strength upper limit, namely, $B_{UpLim} = \frac{B_{G,max}}{\lambda_{max}} \cdot (y_{UpLim} + \lambda_{max} + 1)$, hence, $B_{UpLim} \approx 3770$ G.

Therefore, we finally conclude in the magnetic flux upper limit $\psi_{UpLim} \approx A_{UpLim} \cdot B_{UpLim} \approx 7.23 \times 10^{23}$ Mx. Observations justify this result, since the largest active regions reach a maximum magnetic flux of $\approx 10^{23}$ Mx (Vial 2005, Solanki *et al.* 2006).

7. Discussion and Conclussions

The magnetic flux concentrated in the totality of the granules of the whole area of the quiet Sun (with area $A_{Sun} = 2 \times 10^6$ MSH), having a typical maximum magnetic strength of about $B_G \approx 12$ G (Rabin *et al.* 1991), is equal to $A_{Sun} \cdot B_G \approx 7.2 \times 10^{23}$ Mx (Wang 2004, Fisk 2005). Hence, the upper limit of the magnetic flux in an active region is phenomenologically equal to the magnetic flux concentrated in the totality of the granules of the quite Sun.

Therefore, the magnetic flux concentrated in an active region cannot exceed the magnetic flux concentrated in the photosphere as a whole.

Furthermore, it has to be underlined that the estimated upper limit of the magnetic flux concerns not only the sunspots but also the active regions.

PhMD model concerns the fact of one compact main core of a flux tube, that of an individual sunspot. This is governed by the upper limits of the sunspot photospheric area (photometric factor) and magnetic strength (magnetic factor), as well as by the upper limit of their product, that is of the magnetic flux. Even though, the upper limits of sunspot area and magnetic strength do not indispensably characterize also the host active region, this is thought to hold for the magnetic flux upper limit. Sunspots included in an active region are supposed to be antagonistic in absorbing magnetic flux (inflowing either by solar interior or by local regions), while a dominant sunspot (if there is) shall be the one of outflowing the smaller amount of magnetic flux.

Hence, it is expected that the presence of extremely large sunspots costs the absence of sufficiently smaller ones. As a consequence, it is natural to claim that in the hypothetical presence of the most extended sunspot, attained the areas upper limit, no other sunspot can prevail, as their magnetic flux shall be absorbed by the dominant sunspot. In such a case, all the magnetic flux of the active region has to be transferred to the gigantic sunspot. By means of such consideration we claim that the upper limit for sunspot magnetic flux yields is also an upper limit for active regions.

References

Hathaway, D. H. & Choudhary, D. P. 2005, *NASA Technical Reports Server*, ID: 20050236988

Fisk, L. A. 2005, *ApJ*, 626, 563

Foukal, P. V. 2004, in: *Solar Astrophysics* (Wiley-VCH Verlag GmbH & Co. KGaA,Weinheim), pp. 138-143

Livadiotis, G. & Moussas, X. 2007, *Physica A*, 379, 436

https://doi.org/10.1017/S1743921309029159 Published online by Cambridge University Press

Livadiotis, G. & Moussas, X. 2008, in: G. Contopoulos & P. A. Patsis (eds.), *Chaos in Astronomy* (Springer, Berlin), Ch. 46, p. 455

Livadiotis, G. & Moussas, X. 2009, *Adv. Space Res.*, doi:10.1016/j.asr.2008.09.010, in press

Martínez Pillet, V., Moreno-Insertis, F., & Vázquez, M. 1993, *Astron. Astrophys.*, 274, 521

Rabin, D. M., Devore, C. R., Sheeley, N. R., Harvey, K. L., & Hoeksema, J. T. 1991, in: A. N. Cox, W. C. Livingston & M. S. Matthews (eds.), *Solar Interior and Atmosphere* (The University of Arizona Press), p. 781

Solanki, S. K. 2003, *Astron. Astrophys. Rev.*, 11, 153

Solanki, S. K., Inhester, B., & Schüssler, M. 2006, *Rep. Prog. Phys.*, 69, 563

Vial, J.-C. 2005, *Adv. Space Res.*, 36, 1375

Wang, Y.-M. 2004, *Solar Phys.*, 224, 21